Work from Home and Air Pollution

Nicholas Bloom
nbloom@stanford.edu

Stanford University https://orcid.org/0000-0002-1600-7819

Benjamin Krebs
University of Basel

Joshua Graff Zivin
University of California San Diego jgraffzivin@ucsd.edu https://orcid.org/0000-0002-0820-4900

Matthew Neidell
Columbia University

Social Sciences - Article

Keywords: work from home, air pollution, commuting, mortality

Posted Date: September 17th, 2026

DOI: https://doi.org/10.21203/rs.3.rs-10976734/v1

Additional Declarations: There is **NO** Competing Interest.

Work from Home and Air Pollution

Benjamin Krebs (Basel), Nicholas Bloom (Stanford),
Joshua Graff Zivin (UCSD), and Matthew Neidell (Columbia)

28 August 2026

Abstract: Using satellite-informed data on nitrogen dioxide (NO_2) concentration, we document substantial pollution declines across U.S. metropolitan areas between 2019 and 2025. In the city centers of the 15 largest metropolitan areas, average NO_2 concentrations were 0.9 parts per billion lower in 2025, an 8 percent decline. Reductions were greatest in city centers of large metropolitan areas and smaller in suburbs and less populous metropolitan areas. Across 250 metropolitan areas, higher 2025 work-from-home rates are associated with larger city-center declines relative to outer suburbs. Applying concentration-response estimates from the epidemiological literature, we estimate that this 2025 decline in NO_2 is associated with approximately 1,500 to 3,500 fewer deaths annually.

JEL codes: J2, J3, Q5, R1

Keywords: work from home, air pollution, commuting, mortality

Acknowledgments: We thank the U.S. National Science Foundation, the Smith Richardson Foundation, and Stanford Impact Labs for financial support. Benjamin Krebs acknowledges funding by the Swiss National Science Foundation Grant Number PZ00P1_223786.

Replication files:

https://www.dropbox.com/scl/fo/m762s3otf8fikthiwwcco/AOFWulkVNYCwOOl-bEE5KmEQ?rlkey=5ezqp6lkb5mecxvwur81zsm52&st=310c823v&dl=0

1. Introduction: work from home as an environmental shock

The rise of working from home (WFH) transformed a central feature of economic organization: where workers spend the working day. What began as an emergency response to the COVID-19 pandemic has become a durable feature of modern labor markets. By 2025, roughly 100 million employees in Europe and North America worked schedules that combined home and office days (Aksoy et al., 2025; Buckman et al., 2025). This shift creates potentially large gains: working from home can reduce commuting costs and widen firms' access to talent, with particular benefits for workers facing long commutes, disabilities, or caregiving responsibilities (Pabilonia and Vernon, 2022; Barrero et al., 2023; Davis et al., 2024; Bloom et al., 2026).

The rise in WFH has also substantially reduced commuting, especially into city centers, where employment is concentrated in industries with high WFH rates, including finance, information, and professional services. One important consequence may be improved urban air quality. Transportation is a major source of pollution and, in urban areas, is often the dominant source of ground-level nitrogen dioxide (NO_2) (European Environment Agency, 2026). This is important for health, since exposure to NO_2 is associated with respiratory and cardiovascular disease (U.S. Environmental Protection Agency, 2016). But while WFH may have reduced commuting into city centers, it could have increased local travel near workers' homes, potentially shifting pollution toward suburbs. So, the impact of WFH on pollution is a localized empirical question.

During the 2020 lockdown, there were widely reported city-level improvements in air quality across the U.S. and globally.[1] But did these improvements persist, and how did they differ between city centers and suburbs? This paper studies whether the rise in WFH contributed to long-run changes in urban air pollution overall and by local area. We combine high-resolution monthly satellite-informed estimates of ground-level NO_2 from 2018 to 2025 with ZIP-code-level population data for U.S. metropolitan areas. The fine spatial resolution of the pollution data allows us to examine changes within metropolitan areas. We classify ZIP codes as part of city centers, high-density neighborhoods, suburbs, or outer suburbs and compare changes in NO_2 across these locations before and after the pandemic. We then relate these spatial changes to metropolitan-area WFH shares measured in the Current Population Survey (CPS).

The setting is well suited to distinguishing a persistent WFH effect from the temporary impact of pandemic restrictions. Stay-at-home orders and other emergency measures produced large short-run declines in mobility and pollution in 2020, but those restrictions ended well before 2025. If air quality remained different in 2025 than in 2019, especially in the parts of cities where commuting flows changed most, this would suggest a longer-run effect of WFH and related changes in urban activity. The within-city spatial pattern is central to the analysis: secular improvements in vehicle

[1] For example, Plumer and Popovich (2020), Neil (2020), The Economist (2020).

technology, industrial emissions, or background pollution would tend to affect broad areas, whereas reduced commuting into dense employment centers should produce a sharper decline in central locations than in outer suburbs.

We find large and persistent reductions in NO_2 in many U.S. metropolitan areas. These reductions are concentrated in dense urban locations and are largest in the biggest metropolitan areas. In the 15 largest Metropolitan Statistical Areas (MSAs), city-center NO_2 fell by about 0.9 parts per billion (ppb) in 2025 relative to 2019; reductions were smaller in high-density neighborhoods, suburbs, and outer suburbs. The pattern is not simply a uniform national decline. Dense metropolitan areas such as New York, Los Angeles, Boston, Philadelphia, San Francisco, Seattle, and Washington D.C., experienced large reductions, whereas more decentralized metropolitan areas such as Dallas, Miami, and Phoenix saw smaller improvements and even increases.

Additional evidence points to WFH as an important mechanism. Across metropolitan areas, places with higher WFH shares in 2025 experienced larger declines in city-center NO_2 relative to outer areas. This relationship strengthens as the comparison group is further from the center. Several additional patterns help rule out alternative explanations. The abrupt drop in March 2020 is difficult to reconcile with slower-moving drivers of falling pollution, such as cleaner vehicles or gradual population trends. Similar reductions in heating and non-heating months also weigh against an explanation based on population shifts that reduced domestic gas- and oil-fired heating in city centers.

We also quantify the potential health implications of these pollution changes. Applying standard concentration-response relationships from the epidemiological literature, we estimate that lower NO_2 concentrations in 2025 relative to 2019 are associated with approximately 1,500 to 3,500 fewer annual deaths across U.S. metropolitan areas. While traffic-related NO_2 concentration declined the most in dense metropolitan areas, these estimated mortality reductions are largest in suburbs, because they contain the largest exposed populations.

The broader message is that WFH has environmental consequences as well as workplace consequences. Discussions of WFH often focus on productivity, worker well-being, downtown commercial real estate, public transit, and the future of cities. Our results suggest that air quality and health should also be part of this debate. WFH is not a substitute for clean transportation policy, and some emissions may shift from central cities toward suburban and rural areas. Nevertheless, the evidence indicates that the persistent reduction in commuting to urban employment centers has contributed to meaningful improvements in air quality, with potentially important health benefits.

2. Materials and methods

2.1. Data

Our monthly estimates of average surface-level NO_2 come from the satellite-informed land-use regression dataset developed by Nawaz et al. (2025), which is available on a $0.01° \times 0.01°$ (~1 km × 1 km) grid for the contiguous United States. NO_2 has a short daytime atmospheric lifetime, approximately 5 to 8 hours (Valin et al., 2013), and therefore exhibits substantial spatial variation, making high-resolution estimates particularly valuable. The dataset combines oversampled tropospheric-column NO_2 observations from the Tropospheric Monitoring Instrument (TROPOMI) aboard the Sentinel-5 Precursor satellite with land-use characteristics, ERA5 meteorological reanalysis fields, and ground-level NO_2 measurements from the U.S. Environmental Protection Agency. The only time-varying inputs are satellite NO_2 columns and meteorological reanalysis fields. The land-use component of the model (road and railway density, built environment, population density, water, and elevation) is fixed over time. Concentrations are reported in ppb. We use the publicly available monthly product covering May 2018 through December 2025.[2] For the main analysis, we aggregate the gridded estimates to the ZIP code level using area-weighted averages of all grid cells that overlap each ZIP code.

We measure WFH using all available Basic Monthly samples from the CPS between July 2024 and June 2026, obtained through the Integrated Public Use Microdata Series.[3] We use this two-year window to increase the number of MSAs meeting the threshold of at least 100 observations (see below), but we refer to this measure as the 2025 WFH share throughout the paper. The TELWRKPAY variable identifies whether an employed respondent aged 16 or older teleworked or worked from home for pay during the previous week. We restrict the sample to respondents who were employed and at work during the reference week. We define an indicator equal to one for respondents who worked from home and calculate each MSA's 2025 WFH share as the weighted mean among employed workers, using the CPS final sampling weights (WTFINL). We drop MSAs with fewer than 100 observations.

We use two alternative measures for WFH in complementary results, drawing on datasets constructed and updated using methodologies developed in two earlier papers. First, we examine mentions of hybrid and remote work in job-vacancy postings by county-month, using the methodology developed by Hansen et al. (2023). We aggregate county-level posting shares in 2019 and 2025 to MSAs, weight by the number of postings, and drop MSAs with fewer than 200 postings across the two years. Second, to measure broad industry-level variation in WFH intensity, we use county-level data from the monthly U.S. Survey of Working Arrangements and Attitudes, following the methodology developed by Barrero et al. (2021). Since we use these data at the county level (see below), we do not aggregate them to MSAs.

---

[2] Version 2: https://doi.org/10.5281/zenodo.18919769. Accessed March 10, 2026.
[3] IPUMS CPS variable documentation: https://cps.ipums.org/cps-action/variables/group. Accessed June 8, 2026.

County-level commuting-flow data come from the U.S. Census Bureau's 2016–2020 American Community Survey (ACS) County-to-County Commuting Flows and report the estimated number of workers traveling from each county of residence to each county of work. For each county of work, we sum commuters across all counties of residence to obtain total commuting inflow. We express inflows per km^2 of county land area.

Mortality data come from the Centers for Disease Control and Prevention (CDC) Wide-ranging Online Data for Epidemiologic Research Multiple Cause of Death database.[4] The finest available spatial resolution is the county, so we use county-level crude death rates per 100,000 population, averaged over 2015–2019 to reduce year-to-year noise, and treat rates flagged as unreliable by the CDC as missing. We assign each ZIP code the rate of the county containing the largest share of its population. Where a county rate is missing, we impute the population-weighted MSA mean and, where that is also unavailable, the population-weighted state mean. Multiplying by ZIP-code population yields the baseline number of annual deaths used in Section 5.

Population counts come from Table B01003 (Total Population) of the 2019 ACS five-year Detailed Tables, which we obtain both for ZIP codes and for census tracts.[5] We use the Census Bureau's ZIP Code Tabulation Areas (ZCTAs), polygonal approximations of postal ZIP codes, and refer to them as ZIP codes throughout.

Geographic boundaries come from the Census Bureau's 2010 TIGER/Line shapefiles for ZCTAs, census tracts, counties, and Core Based Statistical Areas, which we restrict to MSAs.[6] We use the 2010 vintage to match the geography underlying the population and mortality data. ZIP codes are assigned to counties and MSAs using the Missouri Census Data Center geocorr2014 crosswalks, based on the county or MSA that contains the largest share of the ZIP code's population.[7] Counties are assigned to MSAs using the Census Bureau's delineation files.[8] Central business district (CBD) coordinates for each MSA are from Holian (2019), as compiled by Ramani et al. (2024).[9] Census tracts enter only where the analysis is at the county level. Because counties are large and unevenly populated, we measure a county's proximity to the CBD as the population-weighted mean distance of its tracts' internal points to the CBD, rather than as the distance from its geographic centroid.

2.2. Methodology

[4] https://wonder.cdc.gov/mcd-icd10.html. Accessed April 2, 2026.
[5] https://data.census.gov/table/ACSDT5Y2019.B01003?q=B01003&g=010XX00US$8600000&y=2019. Accessed May 20, 2026. https://data.census.gov/table/ACSDT5Y2019.B01003?q=B01003:+Total+Population&g=010XX00US$1400000&y=2019. Accessed June 24, 2026.
[6] https://www.census.gov/cgi-bin/geo/shapefiles/index.php. Accessed February 23, 2026.
[7] https://mcdc.missouri.edu/applications/geocorr2014.html. Accessed June 24, 2026.
[8] https://www2.census.gov/programs-surveys/metro-micro/geographies/reference-files/2013/delineation-files/list1.xls. Accessed June 24, 2026.
[9] Since this source does not include Washington D.C., we added it using the coordinates 38.907237, −77.036542.

2.2.1. Sample construction

We begin with all contiguous U.S. ZIP codes in MSAs for which CBD coordinates are available. The resulting sample contains 16,383 ZIP codes in 337 MSAs, with a combined 2019 population of 262 million, or about 80 percent of the 2019 U.S. total. Because the satellite data begin in May 2018, the first full calendar year we observe is 2019, which we use as the pre-pandemic baseline throughout.

The analysis of WFH shares uses a subset of these MSAs. The CPS yields imprecise telework shares in smaller MSAs, so we retain only MSAs with at least 100 usable WFH observations for the period from July 2024 through June 2026. This leaves 250 MSAs for the cross-sectional analysis.

2.2.2. ZIP code classification and MSA size groups

We classify each ZIP code into one of four mutually exclusive categories based on its location relative to the MSA's CBD and its population density, following the procedure in Ramani et al. (2024): Within each MSA, we rank ZIP codes by 2019 population density and classify the top decile as high density, the 50th through 90th percentiles as suburbs, and those below the median as outer suburbs. We then reclassify as city center any ZIP code whose internal point lies within two miles of the CBD coordinates. In MSAs where no ZIP code falls within two miles, we assign the single closest ZIP code to the city-center category, so that every MSA contributes one. We conduct all analyses for three MSA size groups by total 2019 population: the 15 largest MSAs, those ranked 16–50, and those ranked 51–337.

2.2.3. Deseasoning

To remove seasonal variation, we deseason the raw NO_2 series in two steps. First, for each ZIP code and year, we subtract that year's mean from each monthly observation to obtain within-year deviations, excluding 2020 because the collapse in concentrations that spring would distort the estimated seasonal pattern. Second, for each ZIP-code-by-calendar-month cell (e.g., all Januarys in ZIP code 10001), we average these deviations across all available years to estimate the typical seasonal effect, and subtract it from the raw monthly concentration in every year, including 2020. Figure S1 shows the estimated seasonal pattern being removed. The resulting series retains changes in annual mean concentrations while removing recurring monthly patterns.

Figures 1 and 2 map raw concentrations on the native 0.01° × 0.01° grid, without aggregation to ZIP codes. Deseasoning is confined to Figure 3. The remaining analyses compare 2019 with 2025 over balanced sets of months, so the estimated seasonal effect enters both years identically and is differenced out.

2.2.4. Estimating the 2019–2025 change in NO_2

We estimate the change in pollution for all ZIP codes in all MSAs by regressing NO_2 in ZIP code z and month m on an indicator for observations in 2025:

$$NO_{2zm} = \beta\ 2025_{zm} + \iota_z + \varepsilon_{zm} \quad (1)$$

where ι_z denotes ZIP code fixed effects. The estimation sample is restricted to 2019 and 2025, so β captures the average difference in concentrations between those years. Regressions are weighted by 2019 ZIP code population, and standard errors are clustered at the MSA level.

To obtain estimates for a given MSA size and ZIP code density group, we augment equation (1) with an interaction between the 2025 indicator and an indicator for that group, estimated on the full sample of ZIP codes:

$$NO_{2zm} = \beta\ 2025_{zm} + \delta\ (2025_{zm} \times \text{group}_z) + \iota_z + \varepsilon_{zm} \quad (2)$$

The group's own 2019–2025 change is $\beta + \delta$, which we report together with the standard error of that sum. The group indicator itself is absorbed by the ZIP code fixed effects. Each reported estimate uses all ZIP codes, and the remaining ZIP codes serve as the reference group. We further apply the same procedure separately to the 15 largest MSAs, restricting the sample to those MSAs and defining groups by MSA and density category. Because standard errors are clustered at the MSA level, they cannot be reported for single-MSA estimates.

To assess whether reduced domestic heating can account for the city-center decline, we re-estimate equation (2) in logs with a full set of interactions between the 2025 indicator, the group indicator, and an indicator for the non-heating season, which we define as June 1 through September 30; the heating season is October 1 through May 31. We report the implied change for each season in log points, together with the difference between them.

2.2.5. Work from home and the relative city-center decline

To relate pollution changes to WFH, we first average concentrations within ZIP code and year for 2019 and 2025, then aggregate to population-weighted means by MSA and density category, and take the 2025 minus 2019 difference. For each MSA, we form the gap between the city-center change and the change in high-density ZIP codes, suburbs, and outer suburbs, and regress it on the MSA's 2025 WFH share:

$$\Delta NO_{2\text{center},i} - \Delta NO_{2\text{comparison},i} = \gamma\ WFH_i + \alpha + \eta_i \quad (3)$$

Regressions are weighted by 2019 MSA population and use robust standard errors. The number of MSAs is 241 in the high-density specification, since some MSAs have no ZIP codes in that category, and 250 in the other two. Because the CPS telework measure is unavailable before 2020 and pre-pandemic WFH rates were low, we use the 2025 level as a proxy for the post-pandemic increase. We repeat the exercise with the 2019–2025 change in the share of job postings mentioning WFH in place of the CPS share.

2.2.6. County-level measures of commuting exposure and WFH intensity

We relate county-level commuting inflow and WFH-intensive employment, plotting the values and a quadratic fit by distance to the MSA's CBD for counties in the 15 largest MSAs. For commuting inflow, we use a log scale, and for WFH intensity, we use levels.

2.2.7. Mortality implications

We translate estimated pollution changes into mortality using the standard health-impact function implemented in the U.S. Environmental Protection Agency's Environmental Benefits Mapping and Analysis Program Community Edition (BenMAP-CE) framework (Sacks et al., 2018):

$$\Delta \text{Deaths} = \text{Deaths}_0 \times (1 - \exp(\alpha(\beta + \delta))) \quad (4)$$

where Deaths_0 is the baseline number of annual deaths in the exposed population, $\beta + \delta$ is the estimated change in annual NO_2 concentration in µg/m^3, and $\alpha = \ln(1.02)/10$ per µg/m^3 corresponds to a hazard ratio of 1.02 per 10 µg/m^3 increase in long-term NO_2 exposure for all-cause mortality, taken from the World Health Organization-commissioned meta-analysis underlying the 2021 Air Quality Guidelines (Huangfu and Atkinson, 2020). We apply the function separately by ZIP code density and MSA size group. Deaths_0 is the sum across ZIP codes (in a given group) of the 2019 population multiplied by the assigned county mortality rate, as described in Section 2.1, and $\beta + \delta$ is that group's estimated change in NO_2 concentration from equation (2). Coefficients are estimated in ppb and converted to µg/m^3 using 1 ppb = 1.88 µg/m^3, the conversion for NO_2 at 25°C and 1 atmosphere. We report a range obtained by applying the function to the lower and upper bounds of the 95 percent confidence interval around the estimated NO_2 change, rounded to the nearest ten deaths. For MSA-specific results, we report point estimates only. This range reflects statistical uncertainty in the estimated change in NO_2 concentrations but not uncertainty in exposure measurement or in the concentration-response relationship.

3. Post-pandemic change in NO_2 pollution

Figure 1A maps average NO_2 concentrations in the New York and Philadelphia area in 2019. Concentrations exceed 12 ppb in central New York City, more than twice the World Health Organization's recommended annual average guideline of 10 µg/m^3, or about 5.3 ppb at our 1.88 conversion (World Health Organization, 2021). Concentrations decline sharply with distance from the urban core, falling below 3 ppb in the most peripheral areas. This gradient is consistent with transportation being a major urban source of NO_2 (European Environment Agency, 2026). Figure 1B maps the March–May change from 2019 to 2020. Concentrations fell by more than 3 ppb in some central locations, coinciding with lockdown-related reductions in travel (Archer et al., 2020).

Figure 1C maps the change from 2019 to 2025. Even five years after the 2020 lockdown began, NO_2 remained visibly lower in the urban core, falling by as much as 2 ppb in central and Lower Manhattan. By contrast, concentrations increased in some outer-suburban and rural areas.

Looking beyond New York City and Philadelphia, Figure 2 shows that the relative city-center decline from 2019 to 2025 appears across many of the 15 largest U.S. MSAs and their adjacent populous cities.[10] Relative declines are visible in Atlanta, Baltimore, Boston, Chicago, Detroit, Fresno, Houston, Long Beach, Los Angeles, Milwaukee, Oakland, Portland, Riverside, Sacramento, San Diego, San Francisco, San Jose, Seattle, and Washington D.C. No comparable city-center decline occurs in Arlington, Dallas, Fort Worth, Miami, and Phoenix.

Figure 3 shows that the relative decline in city centers also appears across a broader set of U.S. MSAs. We plot monthly deviations in NO_2 concentrations, measured in ppb, from each group's 2019 average. The series are shown separately for city centers, high-density areas, suburbs, and outer suburbs. In Panel A, covering the 15 largest MSAs, NO_2 falls sharply at the onset of lockdowns and then partly recovers, but it remains visibly below its 2019 level through the end of the study period. Before March 2020, the four lines move in synchrony; throughout the post-pandemic period, the decline is ordered by density: it is strongest in city centers, somewhat less in the remaining high-density ZIP codes, and smallest in suburbs and outer suburbs, which stay closest to their 2019 baseline.

Panel B of Figure 3 covers MSAs ranked 16–50, where the same pattern holds but in muted form: the initial drop is smaller, and the separation between lower- and higher-density ZIP codes is narrower, though the ordering is the same. In Panel C, covering MSAs ranked 51–337, the pattern is almost absent. The four density groups move together, dip only briefly at the onset of lockdowns, and return close to their 2019 level, with a modest spread across density groups emerging only toward the end of the study period. Smaller MSAs experienced less separation, in part because pre-pandemic commutes were shorter and their employment was less concentrated in WFH-intensive finance, information, and professional-services industries (Ramani et al., 2024).

Table 1 estimates these changes in a regression framework (Equations (1) and (2) in Section 2.2.4), reporting the estimated change separately for each ZIP code density and MSA size group. Consistent with the figures, Table 1 shows large and statistically significant reductions in NO_2. Across all ZIP codes, concentrations declined by 0.32 ppb relative to their 2019 average. The reduction increases with MSA size, at 0.47 ppb in the top 15 and 0.35 ppb in MSAs ranked 16–50, compared

[10] Figures 1 and 2 plot the 15 largest MSAs and all top-50 cities within their proximity. If a panel does not show any top-50 city, none falls within the frame.

with only 0.11 ppb in MSAs ranked 51–337. Within MSAs, reductions increase with ZIP-code density, though the gradient flattens as MSAs get smaller: in the top 15 MSAs, city centers fell by 0.87 ppb against 0.30 ppb in outer suburbs, whereas in MSAs ranked 51–337 the corresponding declines are 0.19 ppb and 0.04 ppb.

Table 2 reports estimates for each of the 15 largest MSAs.[11] The largest total reductions are in Los Angeles, at 1.17 ppb, followed by New York at 0.81 ppb, Philadelphia at 0.70 ppb, Washington D.C. at 0.67 ppb, and San Francisco at 0.60 ppb. These MSAs also exhibit a particularly steep city center–outer suburb gradient in levels: in Washington D.C., city-center NO_2 fell by 1.28 ppb against 0.37 ppb in outer suburbs, in Los Angeles by 1.65 ppb against 0.92 ppb, and in Philadelphia by 1.14 ppb against 0.50 ppb. Consistent with the pattern seen in Figures 1 and 2, we find that city-center concentrations declined in all but Dallas, Miami, and Phoenix.

4. Work from home and pollution

One explanation for these persistent reductions is the rise in WFH, which increased from approximately 7 percent of paid workdays in 2019 to 60 percent at its 2020 peak, before stabilizing near 25 percent by 2025 (Barrero et al., 2023; Buckman et al., 2025). Figure 4 plots, for each of 250 MSAs, the 2019–2025 change in city-center NO_2 relative to outer suburbs against the MSA's 2025 WFH share from the CPS, the share of employed workers who did any paid work from home during the reference week (Equation (3) in Section 2.2.5).

The figure shows a strong, statistically significant cross-sectional association: MSAs with higher WFH shares experienced larger relative declines in city-center NO_2. The red line corresponds to the regression in column 3 of Table S1, where a 10 percentage point higher WFH share is associated with a 0.20 ppb larger decline in city-center NO_2 relative to outer suburbs (−1.999, SE 0.437), close to the average relative decline across MSAs of 0.23 ppb. The association remains statistically significant when city centers are compared with suburbs (−1.108, SE 0.341) and even with high-density ZIP codes (−0.723, SE 0.256), although it weakens as the comparison group moves closer to the center.

Figure S2 repeats this exercise for 333 MSAs using an alternative WFH measure, the MSA-wide share of job postings mentioning WFH. Because postings data are available before the pandemic, this measure does not rely on the absolute 2025 CPS share and instead allows us to use the 2019–2025 change in WFH, mirroring the construction of our pollution measure. The association is similar in magnitude: a 10 percentage point larger increase in the WFH posting share is associated with a 0.24 ppb larger relative decline in city-center NO_2 (−2.376, SE 0.671).

WFH should reduce NO_2 particularly strongly in city centers for two reasons. First, commuting destinations are far more concentrated near CBDs. In the largest MSAs, commuting inflows per

[11] Note that we do not report the nearby cities shown in Figure 2.

km^2 are roughly 150 times larger in counties within 10 km of the CBD than in counties more than 50 km away (Figure 5A). Second, employment near CBDs is concentrated in industries with high post-pandemic WFH rates (Figure 5B). Counties near CBDs have larger shares of employment in finance, information, and professional services (Ramani et al., 2024), which have higher levels of WFH (Hansen et al., 2023). In contrast, more distant counties are more concentrated in retail, health care, education, and manufacturing, where WFH is less feasible. This generates a clear negative relationship between WFH intensity and distance to the city center.

Together, the concentration of commuter destinations and WFH-intensive employment near CBDs implies a larger post-pandemic reduction in commuting-related travel to city centers than to suburban and rural areas. These forces are especially pronounced in dense MSAs such as New York, Boston, Philadelphia, San Francisco, and Washington D.C., the cities that also saw some of the largest city-center reductions in NO_2 pollution.

5. Quantifying the health implications of reduced pollution

We next estimate the potential health implications of these changes by combining our estimated NO_2 reductions with a concentration-response function for long-term NO_2 exposure and all-cause mortality (Huangfu and Atkinson, 2020) and with baseline county-level mortality rates (Equation (4) in Section 2.2.7).

Table 1 reports estimates for the 15 largest MSAs, MSAs ranked 16–50, MSAs ranked 51–337, and all MSAs. The estimated reductions in NO_2 correspond to approximately 600–2,100, 400–1,100, and 200–500 fewer deaths per year in the three MSA size groups, respectively. Most averted deaths occur in suburbs rather than in city centers, even though the largest concentration declines occur in the densest ZIP codes. Across all MSAs, suburbs account for roughly 800–1,900 averted deaths per year, high-density ZIP codes for 300–700, and outer suburbs for 200–700, against only 100–200 in city centers, while the estimated NO_2 decline is smaller in suburbs (0.33 ppb) and outer suburbs (0.20 ppb) than in high-density ZIP codes (0.49 ppb) and city centers (0.40 ppb). The difference is driven by the size of the exposed population: suburban ZIP codes are home to 141.3 million people in our sample, more than ten times the 12.8 million living in city-center ZIP codes; outer suburbs and high-density ZIP codes add a further 71.2 and 36.9 million, respectively. Across all 337 MSAs, which contain about 80 percent of the 2019 U.S. population, the estimated decline in NO_2 is associated with approximately 1,500–3,500 fewer deaths per year.

Table 2 reports the same calculations for each of the 15 largest MSAs. New York and Los Angeles dominate the aggregate, with roughly 420 and 360 averted deaths per year, together accounting for more than half of the estimated total across the 15 largest MSAs. This reflects both large concentration declines (0.81 ppb and 1.17 ppb) and their large populations of 19.3 and 13.2 million. The suburban concentration of health benefits is visible city by city: in New York, suburbs and high-density ZIP codes account for 210 and 120 averted deaths against 10 in the city center, even though the city-center decline was 1.00 ppb. Dallas and Phoenix instead show higher NO_2 in 2025 than in 2019 across all density groups (0.24 ppb and 0.43 ppb), implying roughly 40 and 60 additional deaths per year.

6. Discussion and conclusion

We find that NO_2 concentrations fell substantially across U.S. metropolitan areas between 2019 and 2025, with the largest reductions in dense urban centers. In the 15 largest MSAs, city-center NO_2 declined by about 0.9 ppb, or 8 percent, relative to 2019. These reductions were not distributed evenly across space: they were larger in city centers than in suburbs and outer suburbs, and larger in the biggest metropolitan areas than in smaller ones. The spatial pattern is consistent with a persistent reduction in commuting to central employment districts rather than a uniform national decline in pollution.

Several pieces of evidence point to WFH as an important contributor to these changes. MSAs with higher WFH shares experienced larger declines in city-center NO_2 relative to outer suburbs, and this association is also present when WFH is measured using job postings that mention remote or hybrid work. This interpretation is further supported by the geography of commuting and employment: counties near CBDs receive much larger commuting inflows and have higher concentrations of industries in which WFH is common.

Our results also help place the post-pandemic rise of WFH in the broader literature on telework and air pollution. Earlier studies examine either pre-pandemic telework, when working from home was relatively uncommon, or the pandemic period itself, when changes in mobility reflected emergency restrictions. Giovanis (2018) found that pre-pandemic teleworking in Switzerland reduced traffic and air pollution, while Bañuelos-Gimeno et al. (2024) found that telework was associated with improved air quality in Madrid during the pandemic period. By contrast, Briole and Lavaine (2026) find that pandemic-induced WFH increased $PM_{2.5}$ in France, as higher residential emissions outweighed lower transport emissions. We study 2025, after lockdowns and other emergency measures had ended and WFH had stabilized as a standard feature of many jobs. We also focus on NO_2, which dissipates within hours and is therefore more geographically localized to emission sources than $PM_{2.5}$ (Costa et al., 2014), allowing us to examine the within-city geography of work and air quality.

Alternative explanations are possible but they cannot fully explain our results. Cleaner vehicle technologies and tighter emissions standards have contributed substantially to long-run reductions in traffic-related air pollution (McDonald et al., 2013; Henneman et al., 2021). These changes are gradual, however, and should reduce emissions broadly across MSAs rather than primarily in city centers. They are therefore unlikely to explain any of the three features of our results: the sharp relative decline in city centers around 2020, the much larger reductions observed in city centers than in suburban areas, and the pronounced cross-city association between these spatial differences and WFH rates.

The decline and relocation of pollution-intensive industrial activity have also contributed to long-run improvements in air quality, alongside tighter environmental regulation and cleaner production technologies (Cherniwchan, 2017; Shapiro and Walker, 2018; Choi et al., 2025). These trends are likewise gradual and broad-based, and so cannot account for any of the three features described above.

Population has shifted away from city centers, partly in response to WFH (Ramani et al., 2024). Lower city-center residential density could reduce emissions from gas- and oil-fired domestic heating, providing an alternative explanation for lower central-city NO_2. We examine this possibility by separating the heating season, which we define as October 1 through May 31 (based on when New York landlords are legally required to provide indoor heat) from the non-heating season, June 1 through September 30.[12] Because gas and oil are often burned locally for space heating, population movement out of city centers could reduce winter city-center NO_2. By contrast, summer air conditioning primarily uses electricity generated at power plants typically located outside city centers. We find similar 2019–2025 declines in heating and non-heating months (Table S2), suggesting that reduced domestic heating cannot account for the city-center decline.

Our analysis builds on recent work that combines high-resolution TROPOMI observations with regulatory monitors and land-use characteristics to estimate ground-level NO_2 at fine spatial resolution (Kim et al., 2024; Nawaz et al., 2025). These products improve substantially on models using earlier satellite instruments, but important uncertainties remain. Satellites measure tropospheric columns rather than surface concentrations, observations are disproportionately available under clear skies, and estimates below the native satellite-pixel resolution depend on statistical downscaling (Kerr et al., 2023; Goldberg et al., 2025). Importantly, the road and land-use predictors in these models are static over time. Only the satellite columns and meteorological reanalysis vary across months, so the temporal variation we exploit does not come from traffic-related model inputs. More specifically, our analysis focuses on within-ZIP-code changes over time, rather than absolute measures of NO_2, so that any time-invariant measurement error should be differenced out.

Estimates of pollution-attributable mortality are sensitive to modeling choices, including spatial resolution, whether exposure is assigned using residential locations alone or both home and workplace locations, and the extent to which the estimates account for confounding (deSouza et al., 2024). We apply the standard BenMAP-CE health-impact framework (Sacks et al., 2018), but the range reported in Table 1 reflects only statistical uncertainty in the estimated NO_2 changes. It does not capture the full uncertainty associated with these other modeling choices, so the mortality estimates should be interpreted as illustrative.

[12] Boston, Chicago, and Philadelphia have similar heating ordinances, suggesting that domestic heating is typically concentrated between October and May.

Overall, our findings are consistent with the rise of WFH contributing to persistent reductions in traffic-related NO_2 across U.S. MSAs, suggesting impacts in addition to its effects on workers, firms, downtowns, transit, and commercial real estate. More broadly, the results demonstrate that changes in the structure of work can have lasting environmental and health consequences by changing commuting behavior. Thus, while WFH is not a substitute for comprehensive transportation or pollution policy, and some emissions may shift geographically, the evidence points to persistent reductions in traffic-related pollution in dense urban centers.

Bibliography

Aksoy, Cevat Giray, José María Barrero, Nicholas Bloom, Steven J. Davis, Mathias Dolls, and Pablo Zarate. 2025. "The Global Persistence of Work from Home." Proceedings of the National Academy of Sciences 122 (27): e2502441122.

Archer, Cristina L., Guido Cervone, Maryam Golbazi, Nicolas Al Fahel, and Carolynne Hultquist. 2020. "Changes in Air Quality and Human Mobility in the USA during the COVID-19 Pandemic." Bulletin of Atmospheric Science and Technology 1: 491–514.

Bañuelos-Gimeno, Jorge, Natalia Sobrino, and Rosa Arce-Ruiz. 2024. "Initial Insights into Teleworking's Effect on Air Quality in Madrid City." Environments 11 (9): 204.

Barrero, José María, Nicholas Bloom, and Steven J. Davis. 2021. "Why Working from Home Will Stick." NBER Working Paper 28731.

Barrero, José María, Nicholas Bloom, and Steven J. Davis. 2023. "The Evolution of Work from Home." Journal of Economic Perspectives 37 (4): 23–49.

Bloom, Nicholas, Gordon B. Dahl, and Dan-Olof Rooth. 2026. "Work from Home and Disability Employment." American Economic Review: Insights 8 (2): 179–195.

Briole, Simon, and Emmanuelle Lavaine. 2026. "Does Working from Home Pollute? The Environmental Effects of WFH." European Economic Review 185: 105266.

Buckman, Shelby R., José María Barrero, Nicholas Bloom, and Steven J. Davis. 2025. "Measuring Work from Home." NBER Working Paper 33508.

Cherniwchan, Jevan. 2017. "Trade Liberalization and the Environment: Evidence from NAFTA and U.S. Manufacturing." Journal of International Economics 105: 130–149.

Choi, Jaerim, Jay Hyun, Gueyon Kim, and Ziho Park. 2025. "The Cleanup of US Manufacturing through Pollution Offshoring." Journal of International Economics 154: 104046.

Costa, Solange, Joana Ferreira, Carlos Silveira, Carla Costa, Diogo Lopes, Hélder Relvas, Carlos Borrego, Peter Roebeling, Ana Isabel Miranda, and João Paulo Teixeira. 2014. "Integrating

Health on Air Quality Assessment—Review Report on Health Risks of Two Major European Outdoor Air Pollutants: PM and NO_2.” Journal of Toxicology and Environmental Health, Part B 17 (6): 307–340.

Davis, Morris A., Andra C. Ghent, and Jesse Gregory. 2024. “The Work-from-Home Technology Boon and Its Consequences.” Review of Economic Studies 91 (6): 3362–3401.

deSouza, Priyanka N., Susan Anenberg, Neal Fann, Lisa M. McKenzie, Elizabeth Chan, Ananya Roy, Jose L. Jimenez, William Raich, Henry Roman, and Patrick L. Kinney. 2024. “Evaluating the Sensitivity of Mortality Attributable to Pollution to Modeling Choices: A Case Study for Colorado.” Environment International 185: 108416.

The Economist. 2020. “Air Pollution Is Returning to Pre-Covid Levels.” September 5, 2020.

European Environment Agency. 2026. “Nitrogen Dioxide—NO_2.” In Air Quality Status in Europe 2026. Copenhagen: European Environment Agency. Published April 30, 2026.

Giovanis, Eleftherios. 2018. “The Relationship between Teleworking, Traffic and Air Pollution.” Atmospheric Pollution Research 9 (1): 1–14.

Goldberg, Daniel L., M. Omar Nawaz, Congmeng Lyu, Jian He, Annmarie G. Carlton, Shobha Kondragunta, and Susan C. Anenberg. 2025. “Clear-Sky and Cloudy-Sky Differences in NO_2 Concentrations over the United States: Implications for Satellite Measurement Applications.” Atmospheric Chemistry and Physics 25: 16287–16302.

Hansen, Stephen, Peter J. Lambert, Nicholas Bloom, Steven J. Davis, Raffaella Sadun, and Bledi Taska. 2023. “Remote Work across Jobs, Companies, and Space.” NBER Working Paper 31007.

Henneman, Lucas R. F., Huizhong Shen, Christian Hogrefe, Armistead G. Russell, and Corwin M. Zigler. 2021. “Four Decades of United States Mobile Source Pollutants: Spatial–Temporal Trends Assessed by Ground-Based Monitors, Air Quality Models, and Satellites.” Environmental Science & Technology 55 (2): 882–892.

Holian, Matthew J. 2019. “Where Is the City’s Center? Five Measures of Central Location.” Cityscape 21 (2): 213–226.

Huangfu, Peijue, and Richard Atkinson. 2020. “Long-Term Exposure to NO_2 and O_3 and All-Cause and Respiratory Mortality: A Systematic Review and Meta-Analysis.” Environment International 144: 105998.

Kerr, Gaige H., Daniel L. Goldberg, Maria H. Harris, Barron H. Henderson, Perry Hystad, Ananya Roy, and Susan C. Anenberg. 2023. “Ethnoracial Disparities in Nitrogen Dioxide Pollution in the United States: Comparing Data Sets from Satellites, Models, and Monitors.” Environmental Science & Technology 57 (48): 19532–19544.

Kim, Eliot J., Tracey Holloway, Ajinkya Kokandakar, Monica Harkey, Stephanie Elkins, Daniel L. Goldberg, and Colleen Heck. 2024. “A Comparison of Regression Methods for Inferring Near-Surface NO_2 with Satellite Data.” Journal of Geophysical Research: Atmospheres 129 (16): e2024JD040906.

McDonald, Brian C., Drew R. Gentner, Allen H. Goldstein, and Robert A. Harley. 2013. “Long-Term Trends in Motor Vehicle Emissions in U.S. Urban Areas.” Environmental Science & Technology 47 (17): 10022–10031.

Nawaz, M. Omar, Daniel L. Goldberg, Gaige H. Kerr, and Susan C. Anenberg. 2025. “TROPOMI Satellite Data Reshape NO_2 Air Pollution Land-Use Regression Modeling Capabilities in the United States.” ACS ES&T Air 2 (2): 187–200.

Neil, Dan. 2020. “Coronavirus Got Rid of Smog. Can Electric Cars Do So Permanently?” Wall Street Journal, April 10, 2020.

Pabilonia, Sabrina Wulff, and Victoria Vernon. 2022. “Telework, Wages, and Time Use in the United States.” Review of Economics of the Household 20 (3): 687–734.

Plumer, Brad, and Nadja Popovich. 2020. “Traffic and Pollution Plummet as U.S. Cities Shut Down for Coronavirus.” New York Times, March 22, 2020.

Ramani, Arjun, Joel Alcedo, and Nicholas Bloom. 2024. “How Working from Home Reshapes Cities.” Proceedings of the National Academy of Sciences 121 (45): e2408930121.

Sacks, Jason D., Jennifer M. Lloyd, Yun Zhu, Jim Anderton, Carey J. Jang, Bryan Hubbell, and Neal Fann. 2018. “The Environmental Benefits Mapping and Analysis Program—Community Edition (BenMAP-CE): A Tool to Estimate the Health and Economic Benefits of Reducing Air Pollution.” Environmental Modelling & Software 104: 118–129.

Shapiro, Joseph S., and Reed Walker. 2018. “Why Is Pollution from US Manufacturing Declining? The Roles of Environmental Regulation, Productivity, and Trade.” American Economic Review 108 (12): 3814–3854.

U.S. Environmental Protection Agency. 2016. Integrated Science Assessment for Oxides of Nitrogen—Health Criteria. EPA/600/R-15/068. Washington, DC: U.S. Environmental Protection Agency.

Valin, Lukas C., Alexander R. Russell, and Ronald C. Cohen. 2013. “Variations of OH Radical in an Urban Plume Inferred from NO_2 Column Measurements.” Geophysical Research Letters 40 (9): 1856–1860.

World Health Organization. 2021. WHO Global Air Quality Guidelines: Particulate Matter ($PM_{2.5}$ and PM_{10}), Ozone, Nitrogen Dioxide, Sulfur Dioxide and Carbon Monoxide. Geneva: World Health Organization.

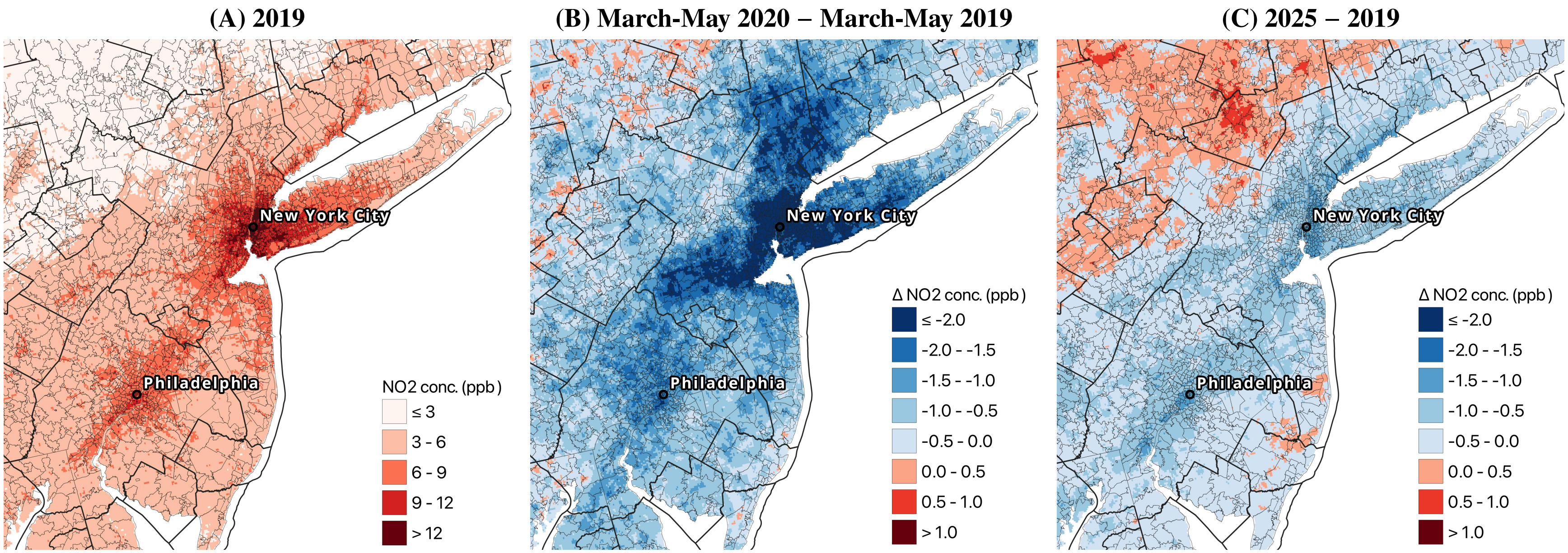

Figure 1: **Average NO_2 levels and their changes in the New York and Philadelphia MSAs and surroundings.** Satellite-informed land-use regression estimates of surface-level NO_2 from Nawaz et al. (2025) in parts per billion (see legends). The spatial resolution is $0.01^\circ \times 0.01^\circ$ (~1 km × 1 km). Circles mark the CBDs of the New York and Philadelphia MSAs. (A) Annual average, 2019. (B) Change in the March-May average, 2020 − 2019. (C) Change in the annual average, 2025 − 2019.

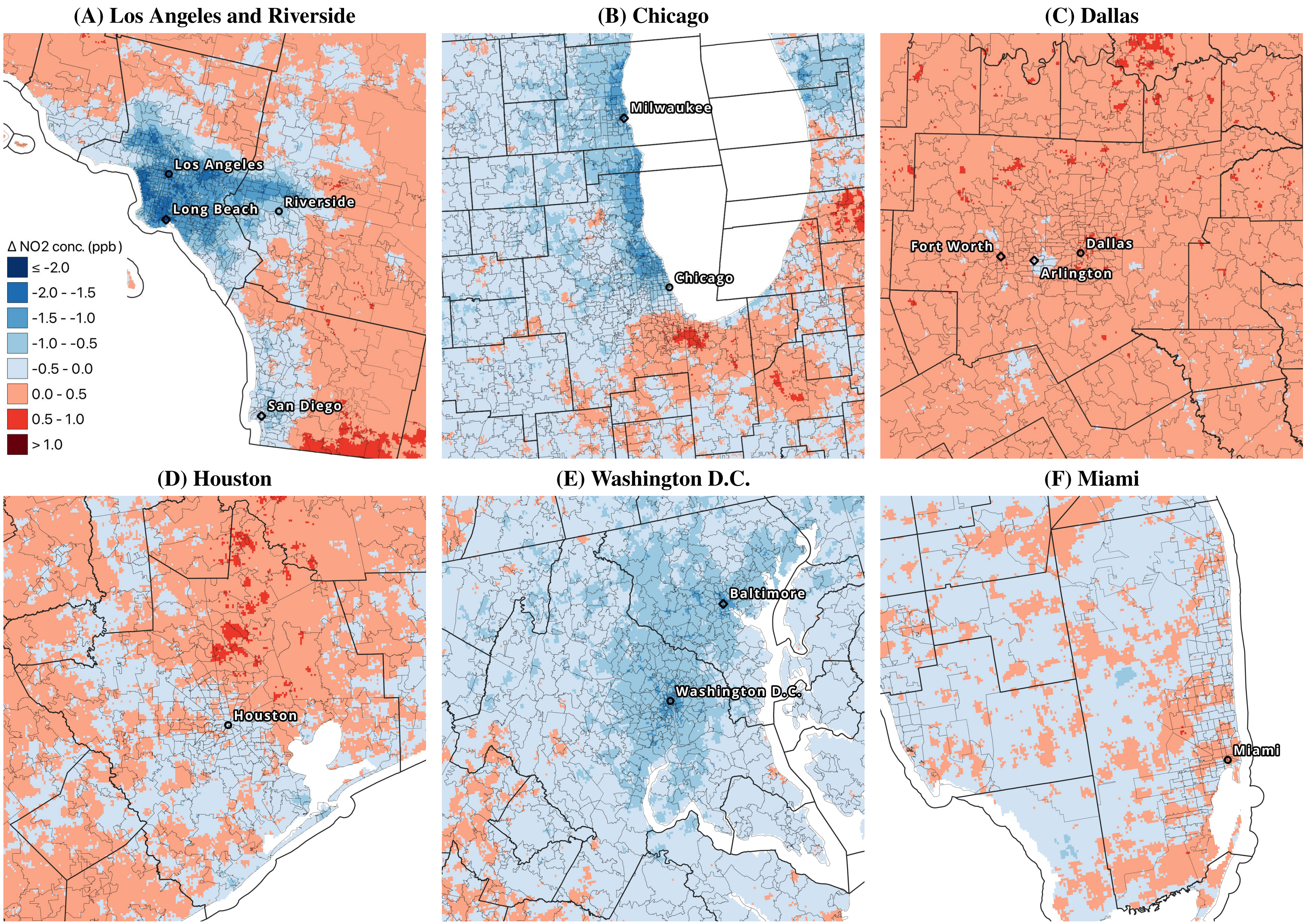

Figure 2: **Change in average NO_2 concentration in the remaining 13 of the 15 most populous MSAs and surroundings, 2025 − 2019.** Satellite-informed land-use regression estimates of surface-level NO_2 from Nawaz et al. (2025) in parts per billion (see legend in (A)). The spatial resolution is $0.01° \times 0.01°$ (~1 km × 1 km). Circles mark the CBDs of these MSAs and diamonds mark the centers of the 50 most populous cities. New York and Philadelphia are excluded, as they are shown in Figure 1. Panels are labeled by MSA; (A) shows the Los Angeles and Riverside MSAs together.

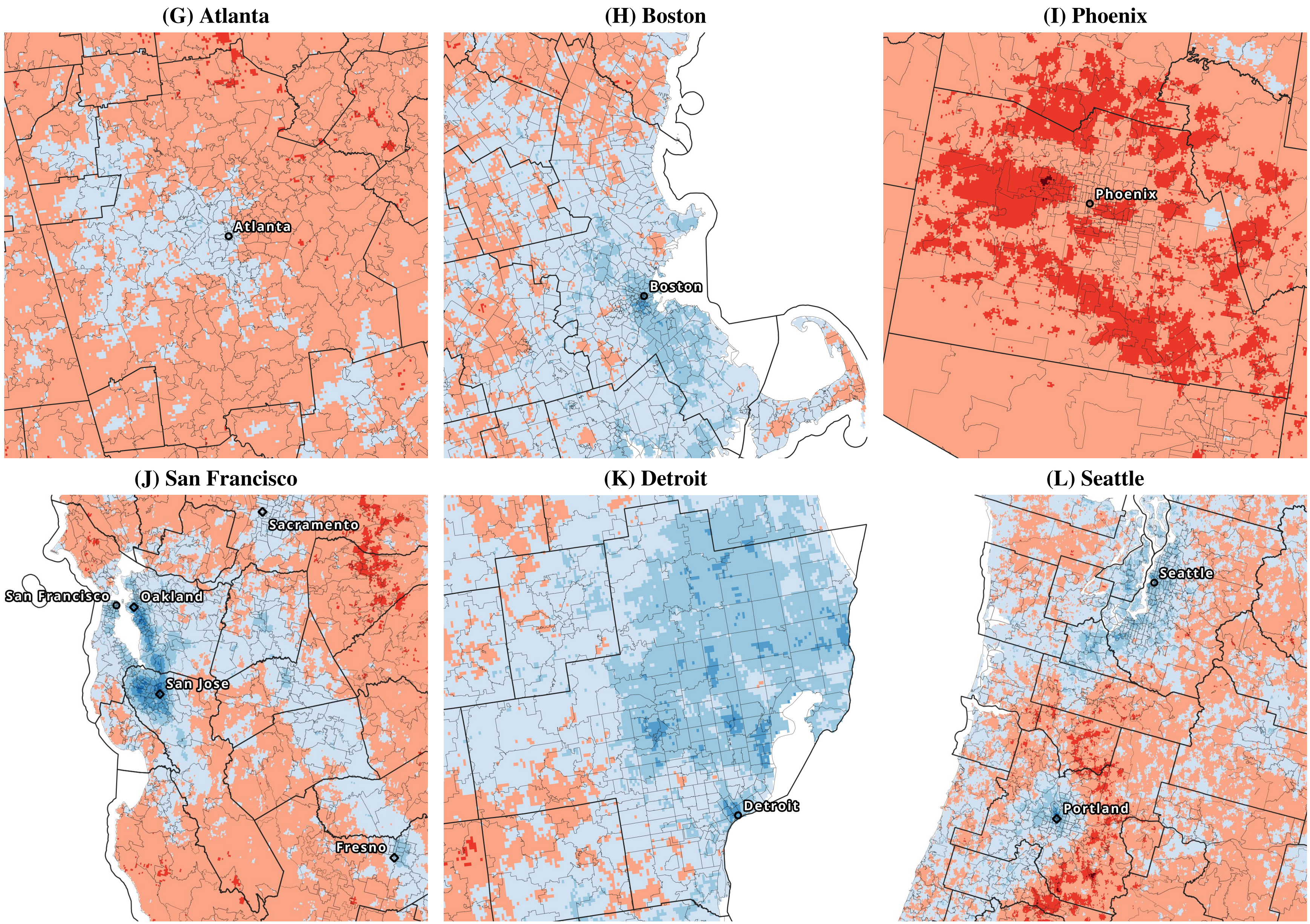

Figure 2: continued.

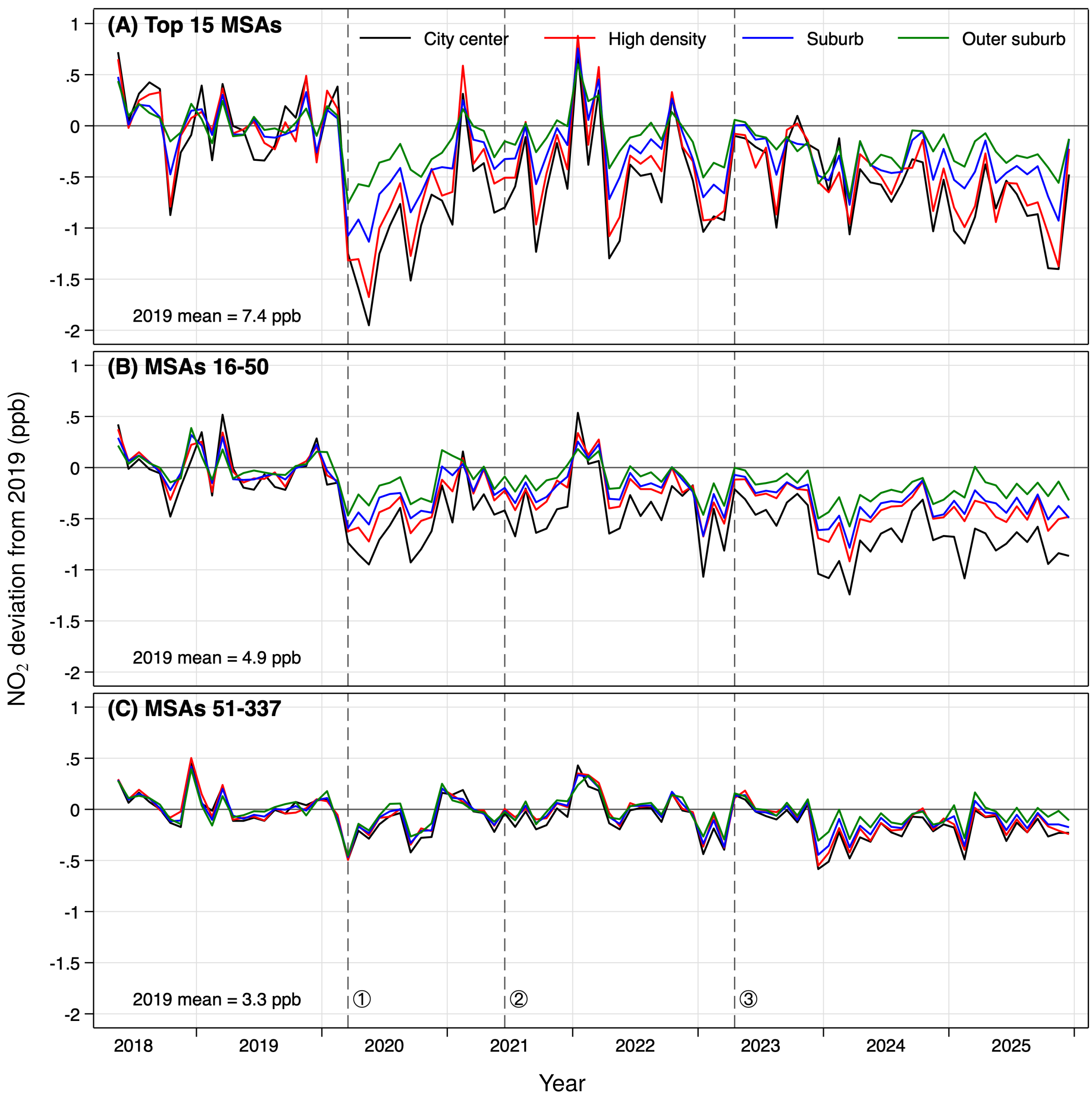

Figure 3: **NO_2 concentration deviations from 2019 levels by MSA size and ZIP code density.** Deviations in parts per billion from each ZIP code's 2019 average, based on deseasoned ZIP-code-level NO_2 concentrations, averaged across ZIP codes within each MSA size and ZIP code density group and weighted by 2019 ZIP code population. Monthly data, May 2018 through December 2025. Lines show city-center (black), high-density (red), suburb (blue), and outer-suburb (green) ZIP codes, defined in Section 2.2.2. The annotation in each panel reports the population-weighted 2019 average across all ZIP codes in that MSA size group. Dashed vertical lines mark: ① Presidential national emergency declaration (March 2020); ② Last statewide stay-at-home order ended (California, June 2021); ③ End of the national emergency declaration (April 2023). (A) Top 15 MSAs. (B) MSAs ranked 16-50. (C) MSAs ranked 51-337.

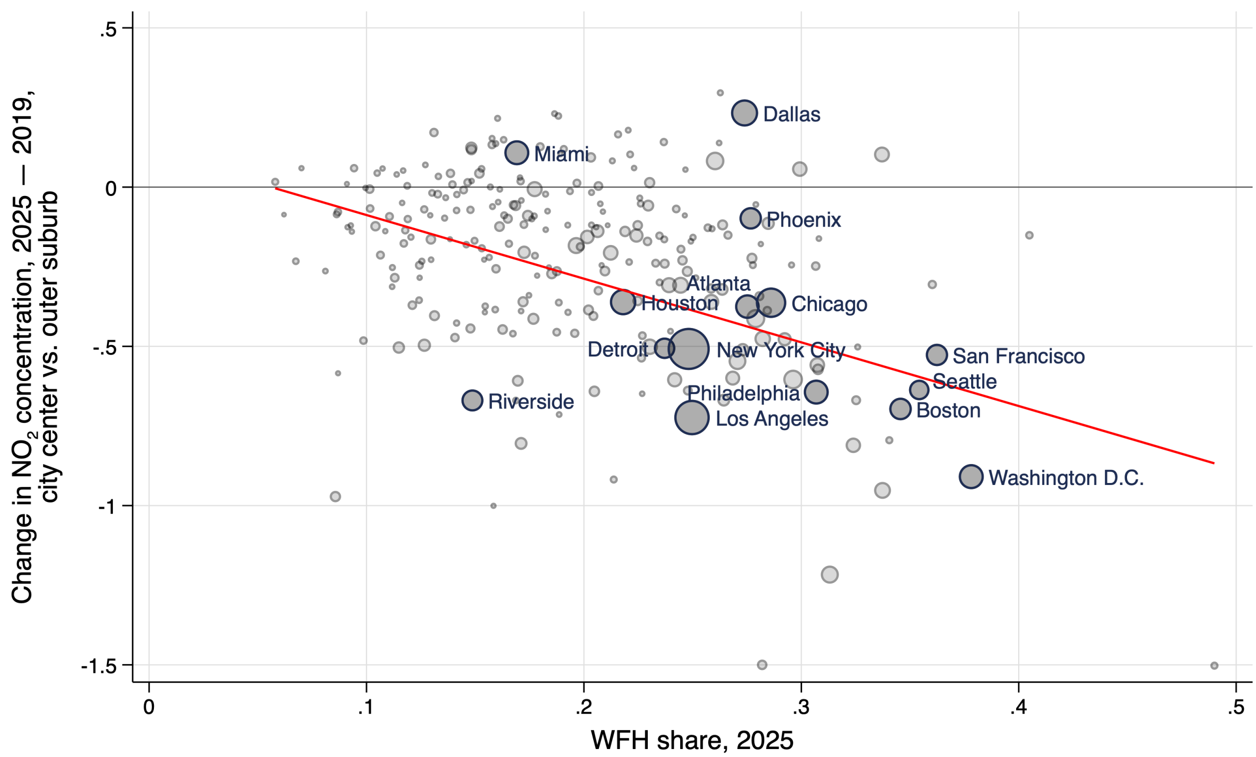

Figure 4: **WFH share and city-center NO_2 change relative to outer suburbs across MSAs.** Each dot represents an MSA, plotting the change in NO_2 concentration, 2025 − 2019, in city-center ZIP codes relative to outer-suburb ZIP codes (vertical axis) against the MSA's 2025 WFH share, the share of employed individuals who did any paid work from home measured in the Current Population Survey (CPS) July 2024 to June 2026 (horizontal axis). Dot sizes are proportional to 2019 MSA population, and the 15 largest MSAs are labeled. The red line is the population-weighted linear fit, corresponding to the regression in column 3 of Table S1. MSAs with fewer than 100 CPS observations between July 2024 and June 2026 are excluded, leaving 250 MSAs.

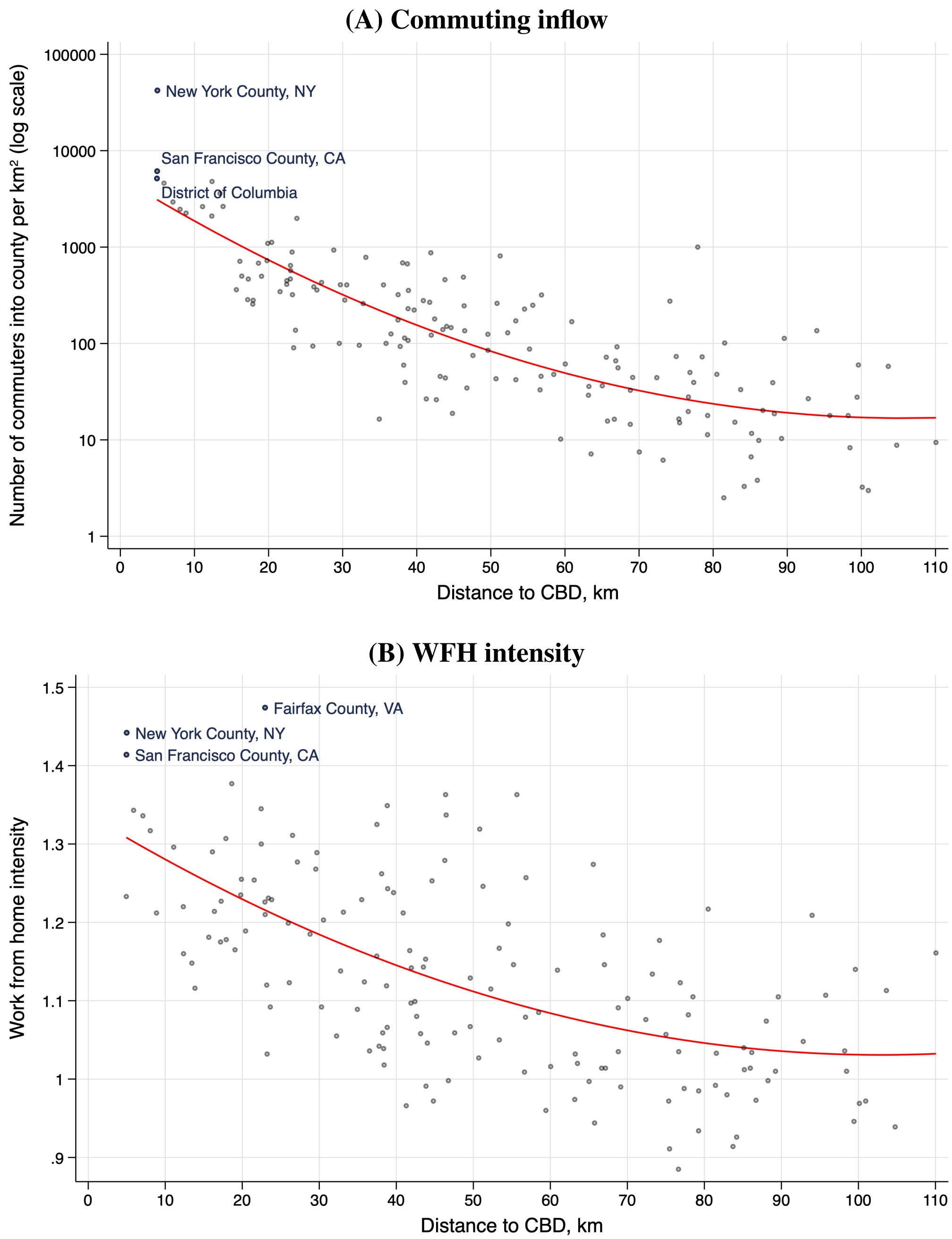

Figure 5: **Commuting inflow and WFH intensity by county distance from the central business district.** Each point represents one of the 155 counties within the 15 largest MSAs. The horizontal axis shows the population-weighted mean distance from the county's census tracts to its MSA's CBD, in kilometers. Selected counties are labeled. (A) Commuting inflow, measured as the number of workers commuting into the county, summed across all counties of residence, per km^2 of county land area, on a log scale. Data are from the 2016-2020 ACS County-to-County Commuting Flows. The red line is a quadratic fit to log commuting inflow, shown in levels. (B) WFH intensity, measured as full-paid days worked from home, from the U.S. Survey of Working Arrangements and Attitudes for March 2025 to February 2026, following Barrero et al. (2021). The red line is a quadratic fit.

Table 1: **Population, NO_2 reductions, and averted deaths by MSA size and ZIP code density.** The table reports total 2019 population in millions, the 2019 average NO_2 concentration, the estimated change in NO_2 concentration in 2025 relative to 2019, all in parts per billion (with standard errors in parentheses), and the implied range of averted annual deaths, for three MSA size and four ZIP code density groups. NO_2 reduction estimates come from regressions of ZIP-code-level NO_2 on a 2025 indicator, with ZIP code fixed effects, weighted by 2019 ZIP code population and with standard errors clustered by MSA. The averted-deaths range is computed by applying the concentration-response function of Huangfu and Atkinson (2020) to the upper and lower bounds of the 95 percent confidence interval on the NO_2 coefficient, combined with each ZIP code's 2019 population and the 2015-2019 average county-level all-cause mortality rate. Averted deaths are rounded to the nearest ten.

		City center	High density	Suburb	Outer suburb	All ZIP codes
Top 15 MSAs	Population	2.2 M	16.4 M	55.6 M	33.2 M	107.4 M
	2019 average NO_2	10.95	10.00	7.67	5.31	7.36
	Δ NO_2 (SE)	-0.87	-0.76	-0.48	-0.30	-0.47
		(0.10)	(0.16)	(0.13)	(0.13)	(0.13)
	Averted deaths	[40; 60]	[180; 450]	[310; 1,060]	[50; 500]	[600; 2,080]
MSAs 16-50	Population	2.1 M	8.7 M	38.5 M	18.7 M	68.0 M
	2019 average NO_2	7.76	6.13	5.07	3.50	4.86
	Δ NO_2 (SE)	-0.76	-0.45	-0.38	-0.20	-0.35
		(0.14)	(0.10)	(0.09)	(0.07)	(0.09)
	Averted deaths	[30; 60]	[70; 170]	[220; 630]	[40; 200]	[370; 1,060]
MSAs 51-337	Population	8.5 M	11.8 M	47.1 M	19.3 M	86.8 M
	2019 average NO_2	4.12	3.89	3.32	2.70	3.33
	Δ NO_2 (SE)	-0.19	-0.16	-0.11	-0.04	-0.11
		(0.03)	(0.03)	(0.02)	(0.02)	(0.02)
	Averted deaths	[40; 70]	[40; 90]	[100; 250]	[0; 60]	[190; 460]
All MSAs	Population	12.8 M	36.9 M	141.3 M	71.2 M	262.2 M
	2019 average NO_2	5.89	7.13	5.51	4.13	5.38
	Δ NO_2 (SE)	-0.40	-0.49	-0.33	-0.20	-0.32
		(0.05)	(0.10)	(0.07)	(0.07)	(0.07)
	Averted deaths	[120; 200]	[310; 740]	[830; 1,890]	[160; 730]	[1,480; 3,540]

Table 2: **Population, NO_2 reductions, and averted deaths for the 15 largest MSAs by ZIP code density.** The table reports total 2019 population in millions, the 2019 average NO_2 concentration, and the estimated change in NO_2 concentration in 2025 relative to 2019, all in parts per billion, together with the implied number of averted annual deaths, for each of the 15 largest MSAs and four ZIP code density groups. MSAs are ordered by 2019 population. NO_2 reduction estimates come from regressions of ZIP-code-level NO_2 on a 2025 indicator, with ZIP code fixed effects, weighted by 2019 ZIP code population. Since we cluster standard errors by MSA, we cannot report them for single MSAs. Averted deaths are computed by applying the concentration-response function of Huangfu and Atkinson (2020) to the NO_2 coefficient, combined with each ZIP code's 2019 population and the 2015-2019 average county-level all-cause mortality rate. Averted deaths are rounded to the nearest ten. Negative values indicate additional deaths.

		City center	High density	Suburb	Outer suburb	All ZIP codes
New York City	Population	0.6 M	4.4 M	9.9 M	4.3 M	19.3 M
	2019 average NO_2	13.29	12.35	9.75	5.84	9.57
	Δ NO_2	-1.00	-1.15	-0.79	-0.49	-0.81
	Averted deaths	10	120	210	70	420
Los Angeles	Population	0.2 M	1.8 M	5.8 M	5.4 M	13.2 M
	2019 average NO_2	16.95	13.93	12.86	9.42	11.65
	Δ NO_2	-1.65	-1.36	-1.32	-0.92	-1.17
	Averted deaths	10	60	180	120	360
Chicago	Population	0.2 M	1.8 M	4.6 M	3.0 M	9.5 M
	2019 average NO_2	13.01	10.49	7.98	5.50	7.76
	Δ NO_2	-0.65	-0.80	-0.43	-0.29	-0.46
	Averted deaths	0	40	60	20	120
Dallas	Population	0.1 M	1.0 M	3.9 M	2.4 M	7.3 M
	2019 average NO_2	9.59	7.17	6.46	4.11	5.82
	Δ NO_2	0.46	0.29	0.23	0.22	0.24
	Averted deaths	0	-10	-20	-10	-40
Houston	Population	0.0 M	0.9 M	3.8 M	2.2 M	6.9 M
	2019 average NO_2	10.47	7.61	6.23	4.14	5.77
	Δ NO_2	-0.31	-0.05	-0.03	0.06	-0.01
	Averted deaths	0	0	0	0	0
Washington D.C.	Population	0.2 M	0.8 M	3.9 M	1.2 M	6.1 M
	2019 average NO_2	10.55	7.77	5.70	3.69	5.71
	Δ NO_2	-1.28	-1.00	-0.66	-0.37	-0.67
	Averted deaths	10	20	50	10	90
Miami	Population	0.1 M	0.7 M	2.9 M	2.4 M	6.1 M
	2019 average NO_2	5.48	5.31	4.27	3.41	4.06
	Δ NO_2	0.06	0.04	-0.06	-0.05	-0.04
	Averted deaths	0	0	0	0	10

Table 2: continued.

		City center	High density	Suburb	Outer suburb	All ZIP codes
Philadelphia	Population	0.2 M	1.1 M	2.8 M	2.0 M	6.1 M
	2019 average NO_2	9.15	8.28	6.93	5.05	6.63
	Δ NO_2	-1.14	-0.94	-0.72	-0.50	-0.70
	Averted deaths	10	40	70	30	150
Atlanta	Population	0.1 M	0.4 M	3.4 M	2.0 M	5.9 M
	2019 average NO_2	8.32	5.88	4.81	3.40	4.43
	Δ NO_2	-0.26	-0.03	0.06	0.11	0.07
	Averted deaths	0	0	0	-10	-10
Boston	Population	0.2 M	0.6 M	2.6 M	1.5 M	4.8 M
	2019 average NO_2	8.06	7.02	5.14	3.30	4.90
	Δ NO_2	-0.96	-0.78	-0.48	-0.26	-0.47
	Averted deaths	0	10	40	10	70
Phoenix	Population	0.0 M	0.7 M	2.5 M	1.6 M	4.8 M
	2019 average NO_2	10.66	8.43	6.72	3.87	6.07
	Δ NO_2	0.37	0.44	0.41	0.47	0.43
	Averted deaths	0	-10	-30	-20	-60
San Francisco	Population	0.3 M	0.4 M	2.4 M	1.6 M	4.7 M
	2019 average NO_2	7.58	7.04	7.49	4.72	6.54
	Δ NO_2	-0.83	-0.70	-0.75	-0.30	-0.60
	Averted deaths	10	10	40	10	70
Riverside	Population	0.0 M	0.8 M	2.9 M	0.9 M	4.6 M
	2019 average NO_2	10.38	11.79	7.24	3.85	7.39
	Δ NO_2	-0.62	-1.04	-0.39	0.05	-0.42
	Averted deaths	0	20	30	0	50
Detroit	Population	0.0 M	0.6 M	2.2 M	1.4 M	4.3 M
	2019 average NO_2	9.85	7.73	6.86	4.53	6.26
	Δ NO_2	-0.97	-0.46	-0.54	-0.46	-0.50
	Averted deaths	0	10	40	20	80
Seattle	Population	0.1 M	0.4 M	2.1 M	1.3 M	3.9 M
	2019 average NO_2	11.11	7.74	7.27	5.19	6.73
	Δ NO_2	-0.97	-0.79	-0.54	-0.33	-0.51
	Averted deaths	0	10	30	10	50

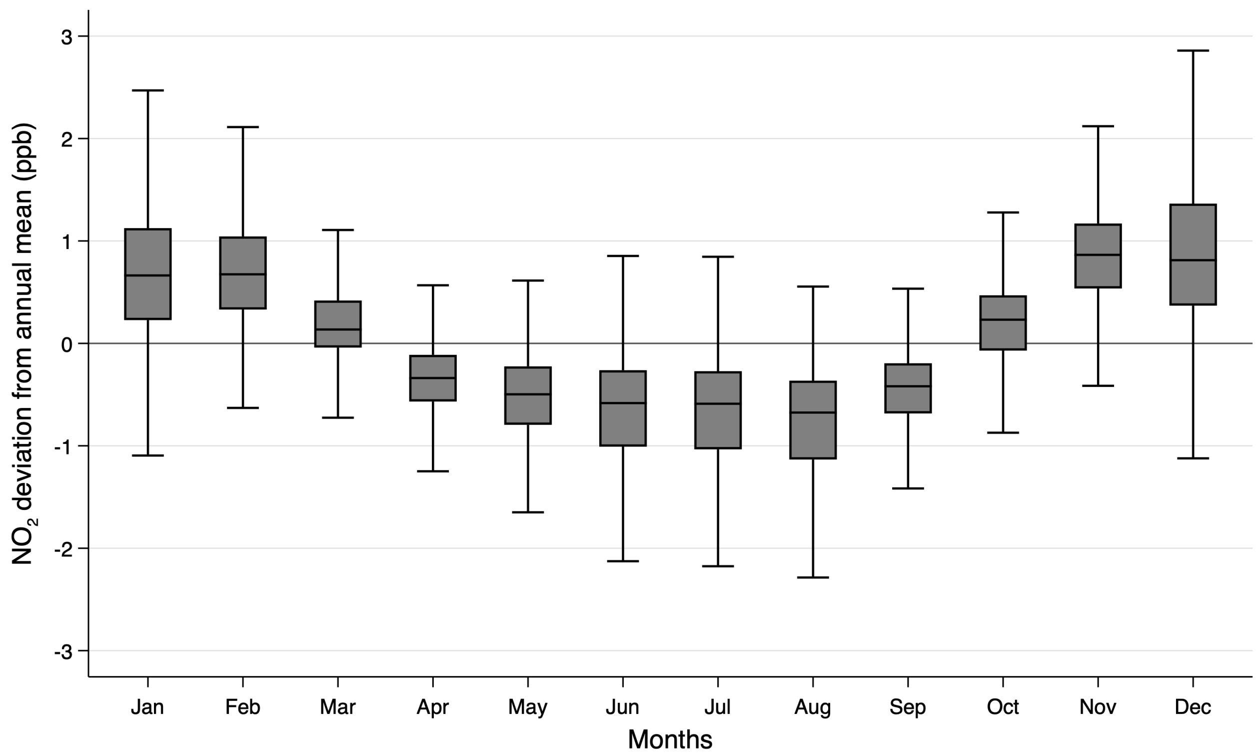

Figure S1: **Seasonal pattern of NO_2 concentrations across ZIP codes.** Distribution across the 16,383 ZIP codes in our sample of the average within-year deviation in NO_2 concentration, in parts per billion, from each ZIP code's annual mean, by calendar month. Deviations are averaged over May 2018 through December 2025, excluding 2020, whose spring collapse in concentrations would distort the estimated seasonal pattern. Boxes show the interquartile range, with horizontal lines marking medians. Whiskers extend to the most extreme non-outlier values, and outliers are not plotted. The figure illustrates the seasonal pattern that is removed from NO_2 concentrations in our deseasoning procedure, which is applied only in Figure 3.

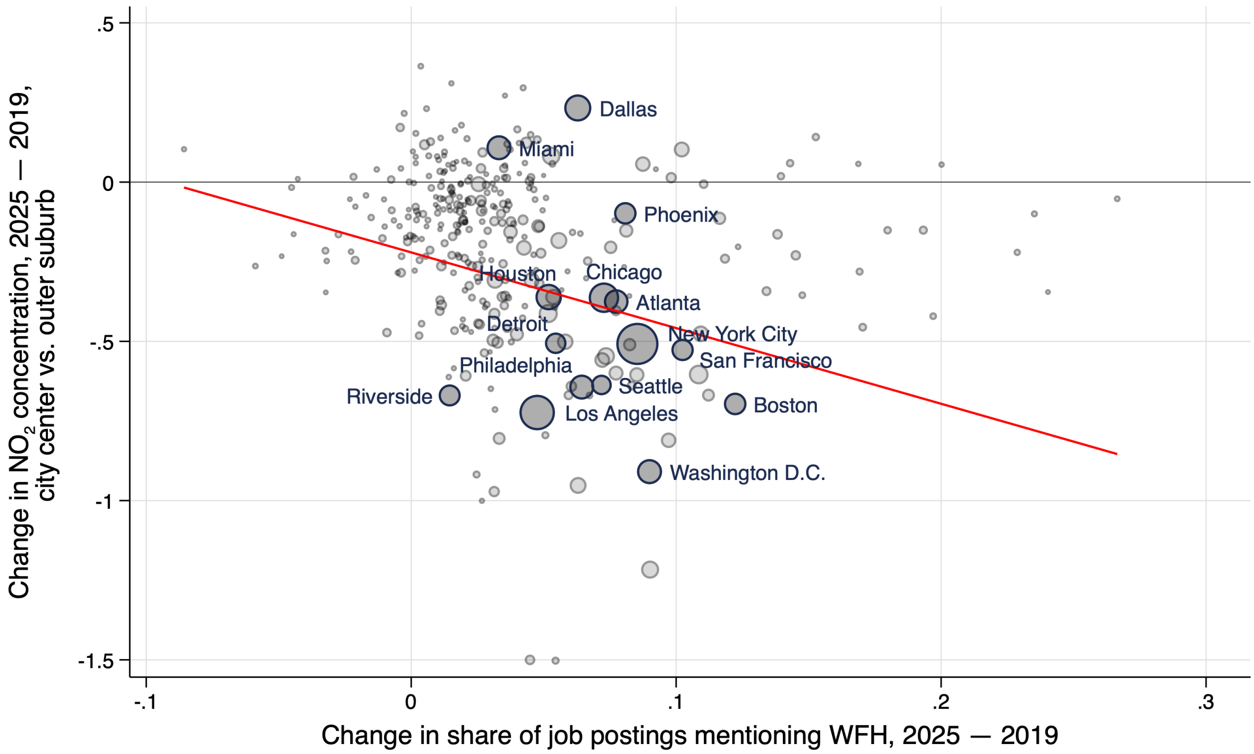

Figure S2: **Change in the share of job postings mentioning WFH and city-center NO_2 change relative to outer suburbs across MSAs.** Each dot represents an MSA, plotting the change in NO_2 concentration, 2025 − 2019, in city-center ZIP codes relative to outer-suburb ZIP codes (vertical axis, as in Figure 4) against the MSA-level change in the share of job postings mentioning WFH, 2025 − 2019 (horizontal axis). Postings data are from Hansen et al. (2023). County-level changes are aggregated to MSAs weighting by the number of postings. Counties with fewer than 200 postings across both years are excluded, leaving 333 MSAs. Dot sizes are proportional to 2019 MSA population, and the 15 largest MSAs are labeled. The red line is the population-weighted linear fit, with a slope of −2.376 (SE 0.671).

Table S1: **Work from home and city-center NO_2 change relative to lower-density areas across MSAs.** The table reports estimates from cross-MSA regressions of the relative change in NO_2 concentration on the MSA WFH share, weighted by 2019 MSA population. An observation is an MSA. The dependent variable is the change in NO_2 concentration in parts per billion, 2025 − 2019, in city-center ZIP codes relative to a comparison density group: high-density ZIP codes (column 1), suburbs (column 2), and outer suburbs (column 3). Group averages within each MSA are weighted by 2019 ZIP code population. The independent variable is the MSA's 2025 WFH share, the share of employed individuals working from home. MSAs with fewer than 100 CPS observations between July 2024 and June 2026 are excluded. Column 1 additionally drops the nine MSAs without a high-density group distinct from the city center. Robust standard errors are reported in parentheses. Column 4 reports the unweighted mean and standard deviation (in brackets) of the WFH share across MSAs. The row labeled "average dependent variable" reports the unweighted mean and standard deviation (in brackets) of the dependent variable across MSAs.

Dependent variable:	Change in NO_2 concentration, 2025−2019, city center vs.			
	high density	suburb	outer suburb	Average WFH share 2025
WFH share 2025	-0.723	-1.108	-1.999	0.197
	(0.256)	(0.341)	(0.437)	[0.072]
Average dependent variable	-0.057	-0.119	-0.227	
	[0.170]	[0.191]	[0.285]	
R^2	0.064	0.137	0.188	
Observations	241	250	250	

Table S2: **NO_2 reductions by season, MSA size, and ZIP code density.** The table reports the estimated change in NO_2 concentration in 2025 relative to 2019, separately for the non-heating season (June 1-September 30) and the heating season (October 1-May 31), for three MSA size and four ZIP code density groups. Estimates come from regressions of log ZIP-code-level NO_2 on a 2025 indicator fully interacted with the density group and a non-heating-season indicator, with ZIP code fixed effects, weighted by 2019 ZIP code population and with standard errors clustered by MSA. Coefficients are in log points and approximate proportional changes. The row labeled "Difference" reports the non-heating-season estimate minus the heating-season estimate. Standard errors are in parentheses.

		City center	High density	Suburb	Outer suburb	All ZIP codes
Top 15 MSAs	Jun-Sep	-0.067	-0.068	-0.056	-0.054	-0.058
		(0.022)	(0.017)	(0.020)	(0.021)	(0.019)
	Oct-May	-0.092	-0.077	-0.060	-0.040	-0.057
		(0.012)	(0.018)	(0.018)	(0.020)	(0.018)
	Difference	0.025	0.009	0.004	-0.014	-0.000
		(0.026)	(0.025)	(0.027)	(0.023)	(0.026)
MSAs 16-50	Jun-Sep	-0.078	-0.062	-0.063	-0.053	-0.061
		(0.015)	(0.012)	(0.012)	(0.014)	(0.012)
	Oct-May	-0.104	-0.070	-0.064	-0.043	-0.060
		(0.017)	(0.016)	(0.019)	(0.026)	(0.020)
	Difference	0.026	0.008	0.001	-0.010	-0.000
		(0.017)	(0.012)	(0.016)	(0.025)	(0.017)
MSAs 51-337	Jun-Sep	-0.033	-0.026	-0.024	-0.021	-0.024
		(0.007)	(0.007)	(0.007)	(0.007)	(0.006)
	Oct-May	-0.040	-0.029	-0.022	0.005	-0.019
		(0.008)	(0.009)	(0.008)	(0.009)	(0.008)
	Difference	0.008	0.003	-0.002	-0.026	-0.006
		(0.010)	(0.009)	(0.010)	(0.011)	(0.009)
All MSAs	Jun-Sep	-0.046	-0.053	-0.047	-0.045	-0.047
		(0.007)	(0.008)	(0.009)	(0.011)	(0.009)
	Oct-May	-0.060	-0.060	-0.048	-0.029	-0.045
		(0.007)	(0.011)	(0.010)	(0.012)	(0.010)
	Difference	0.014	0.007	0.001	-0.016	-0.002
		(0.009)	(0.012)	(0.012)	(0.013)	(0.012)